JOTCS A
Journal of the Turkish Chemical Society
Section: A
Chemistry

TURKISH
CHEMICAL SOCIETY

Exploration of Role of Concentration on Sensing Activities Using Novel Unsymmetrical Schiff Bases

Saranya Dhasarathan, Selvaraj Shunmugaperumal, Kamatchi Selvaraj P*

PG & Research Department of Chemistry, Government Arts College for Men (Autonomous), Nandanam, Chennai-600 035, (Affiliated to University of Madras), Tamil Nadu, India.

Abstract: Simultaneous condensation reaction of thiocarbohydrazide with simple aromatic aldehyde and highly reactive ferrocenecarboxaldehyde resulted in unusual unsymmetrical Schiff bases associated with multi-metal ion sensing property. Spectral characterization methods indicate the formation of the new materials. The guest-host relationship established between various metal ions and receptors changes the electronic spectra drastically, and for the addition of Cu^{2+} ions, the formation of an MLCT charge transfer band around 465 nm, responsible for the coordination of metal ions with receptors, has been noticed. Enhanced ΔE_P (132- 219 mV) values derived from the anodic and cathodic potential data suggested a quasi-reversible process. The various ΔI_{pa} (%) deduced from the I_{pa} amount detected from the recorded responses of applied potential on the different metals added, and metal-free receptor solution, revealed the concentration of metal ions required for the effective sensing process.

Keywords: Azomethine; cation sensors; ferrocene; binding attitude

Submitted: October 13, 2021. **Accepted:** February 28, 2022.

Cite this: Dhasarathan S, Shunmugaperumal S, Kamatchi Selvaraj P. Exploration of Role of Concentration on Sensing Activities Using Novel Unsymmetrical Schiff Bases. Journal of the Turkish Chemical Society Section A: Chemistry. 2022;9(2):465–78.

DOI: https://doi.org/10.18596/jotcsa.1008926.

*Corresponding author. E-mail: porbal96@gmail.com.

INTRODUCTION

Heavy metal ion detection always attracts scientists due to its role in environmental maintenance, catalytic and biological reactions. Steps involved in industrial and agricultural activities keep introducing cations and anions into the environment (1). Instrumental methods of detection of the above ions include high cost, enormous time, and less accuracy (2, 3). Chemosensors decrease the problems faced in instrumental methods by giving selective binding to the ions with detectable changes in response to applied potential, electronic spectral disparity, and emission spectra (4). The ability of Schiff bases to coordinate with metal ions is exploited extensively in sensor development (5-7).

Acquisition of Hg^{2+} ions affects the central nervous system in humans and generates dizziness, disorderliness in sleeping, deformity in limbs and loss of life from over consumption (8-10). Copper is essential for life as it is present in enzymes and proteins responsible for energy production (11). Elevated levels of copper result in Alzheimer's disease, autism, and Tourette's syndrome (12-14). Exposure to nickel initially causes irritation, nausea and vomiting. After some time, victim experiences chest stiffness, palpitation, weakness, and sweating. This may lead to cardiac arrest or respiratory distress syndrome (15-17).

Manganese-containing enzymes control many biological reactions (18). Excessive intake roots to the generation of reactive oxygen species and results in Parkinson's disorder (19-22). Lead, as a poisonous metal adds learning deficits, lowered IQ, and abnormal behavior in children and adult's acquaintance anaemia, increase in blood pressure,

fertility reduction, failure of renal & cerebral function and also loss of life (23-25). Carcinogenesis occurs in kidney, liver, lung, brain, bone, testis, and blood stream by the acquisition of cadmium ions into the biological system (26-28).

The present paper discusses the preparation, characterization, and exploration of the sensing ability of new unsymmetrical Schiff bases. *N*'-((*E*)-4-nitrobenzylidene)-2-((*E*)-2-(ferrocenylidene)hydrazine-1-carbothiohydrazide and *N*'((*E*)-4-*N*,*N*-dimethylaminobenzylidene) -2-((*E*)-2-(ferrocenylidene)hydrazine-1-carbothiohydrazide.

EXPERIMENTAL

Materials

Ferrocenecarboxaldehyde, 4-nitrobenzaldehyde, *p*-dimethylaminobenzaldehyde, carbon disulfide, hydrazine hydrate, and silica gel employed were of analytical grade, from Merck chemical industries. Metal salts (AR grade) like $HgCl_2$, $CuCl_2$, $MnCl_2$, $NiCl_2$, $Cd(OAc)_2$, and $Pb(OAc)_2$ were purchased from Sigma–Aldrich. HPLC grade acetonitrile was acquired from E-Merck and absolute ethanol was obtained from Commercial Alcohols, Canada. Supporting electrolyte tetrabutylammonium perchlorate [99+%] was bought from Chemical Center, Mumbai.

Instruments

Heraeus C-H-N rapid analyzer was used to analyze the C, H, and N contents of the sample. KBr pellets of the sample were loaded into the Perkin-Elmer 337 spectrometer to record the FTIR spectra in the range of 400-4000 cm^{-1}. Shimadzu model UV-1800 240V spectrophotometer was employed to record the UV–visible spectra between 200 and 800 nm wavelength. Proton NMR spectra were recorded on 500 MHz, BRUKER AVANCE spectrometer using C_2D_5OD as the solvent. Bruker Daltonics Esquire 3000 spectrometer was employed to obtain the mass spectra. Responses to the applied potential were observed on CHI electrochemical analyzer 1200B model equipped with platinum wire counter electrode, Ag/AgCl reference electrode, and glassy carbon working electrode.

Synthesis of *N*'-((*E*)-4-nitrobenzylidene)-2-((*E*)-2-(ferrocenylidene)hydrazine-1-carbothiohydrazide [R1]

Refluxing the mixture of 3 moles of hydrazine hydrate and 1 mole of carbon disulfide at 80 ºC in the presence of the catalyst 2- chloroethanol (0.15 mole) for 10 hours yielded thiocarbohydrazide (29). Mixture containing 0.01 mole of 4–nitrobenzaldehyde and 0.01 mole of ferrocenecarboxaldehyde. 180 mL of ethanol were added with stirring (half an hour) to 0.01 mole of purified thiocarbohydrazide in 25 mL of ethanol and then refluxed for 6-7 hours. The reaction mixture was filtered after cooling, then concentrated to get the crude product. Purification of *N*'-((*E*)-4-nitrobenzylidene)-2-((*E*)-2-(ferrocenylidene)hydrazine-1-carbothiohydrazide was carried out in a silica gel column using ethanol as eluent. Color: reddish orange. Yield: 0.5939 g (82%), m.p.180 ºC.

Synthesis of *N*'((*E*)-4-*N*,*N*-dimethylaminobenzylidene)-2-((*E*)-2-(ferrocenylidene) hydrazine-1-carbothiohydrazide [R2]

To a solution of 0.01 mole of thiocarbohydrazide in 25 mL of ethanol, another solution containing 0.01 mole of *p*-dimethylaminobenzaldehyde and 0.01 mole of ferrocene carboxaldehyde in 180 mL of ethanol was added slowly with stirring for half an hour, then refluxed for 6-7 hours. Greenish yellow colored reaction mixture was cooled, filtered, and concentrated to get the crude product. Purification of the crude sample in a silica gel column using ethanol as eluent yielded reddish yellow-colored *N*'((*E*)-4-*N*,*N*-dimethylamino benzylidene)-2-((*E*)-2-(ferrocenylidene)hydrazine-1-carbothiohydrazide [R2]. Yield: 0.5404 g, (91%), Color: Reddish yellow, m.p. 60 °C.

RESULTS AND DISCUSSION

Elemental and Mass Spectral Analysis

Elemental analysis data of the synthesized receptor were in agreement with the theoretically calculated ones, R1- $C_{19}H_{17}N_5O_2SFe$ (%): C, 50.61; H, 3.73; N, 15.51; Fe, 12.18. R2 - $C_{21}H_{23}N_5O_2SFe$ (%): H, 5.32; C, 58.30; N, 16.23; Fe, 12.70. Mass spectra of the compounds R1 and R2 contained molecular peaks at (ESI) m/z 434 and 434, respectively, which ascertain the formation of anticipated material.

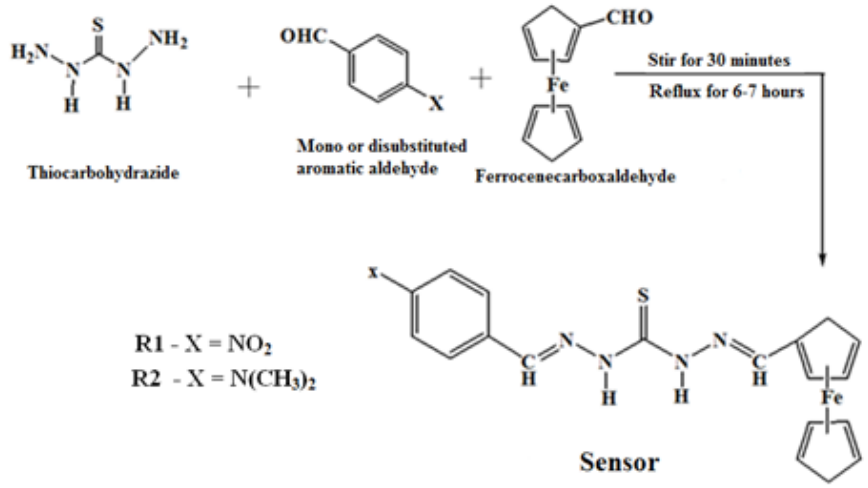

Scheme 1: Synthesis of the sensor molecule.

Vibrational Assignment

The ferrocene cyclopentadienyl ring's tilt stretching vibration and C-H out of plane bend vibrations of R1 appeared as peaks of about 479 cm^{-1} and 816 cm^{-1}, respectively (30). The δ-C-C-H bending vibration in the pentacyclic ring emerged near 933 cm^{-1}. The 1104 cm^{-1} peak was fixed for ring breathing vibration (31). The C=S group stretching vibration, C-C stretching vibration of pentacyclic ring and NO_2 group vibration arises at 1336 cm^{-1}, 1514 cm^{-1} and 1566 cm^{-1} respectively. The Schiff base development is authorized by the appearance of –C=N stretching vibration peak at 1650 cm^{-1}(30). The aromatic stretching vibration transpired at 2064 cm^{-1}. Stretching vibration due to secondary amine and hydration water became apparent around 3360 - 3400 cm^{-1}. Stretching vibrational modes of CH_3 groups present in R2 became obvious near 2916 cm^{-1}(32) along with all other peaks appeared for R1 .

NMR Spectral Analysis

Receptor R1 proton NMR spectrum (Figure 2) in C_2D_5OD possess pertinent peaks and are earmarked as given here - **R1**: 8.2 (s, 2H, NCH), 7.9 (m, 4H aromatic), 4.9 (m, 2H, cp subst.) 4.4(m, 2H, cp subst.) 4.3(s, 5H, cp unsubst.), 1.2(s, 2H, 2NH) **R2**: 8.1(s, 2H, NCH), 7.4 (m, 2H, aromatic), 6.7(d, 2H, aromatic), 4.7 (m, 2H, cp subst), 4.5(m, 2H, cp subst), 4.2 (s,5H, cp unsubst), 3.0 (s,6H, $N(CH3)_2$), 1.1(s, 2H, 2NH).

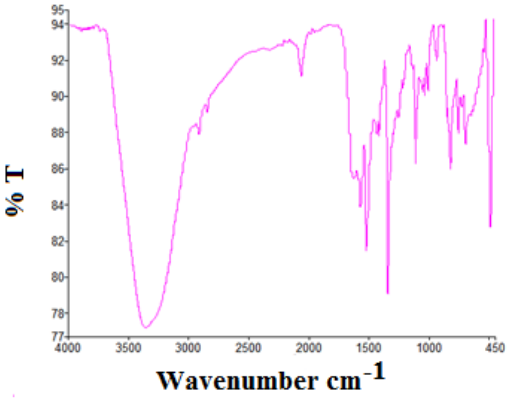

Figure 1: FTIR spectrum of R1.

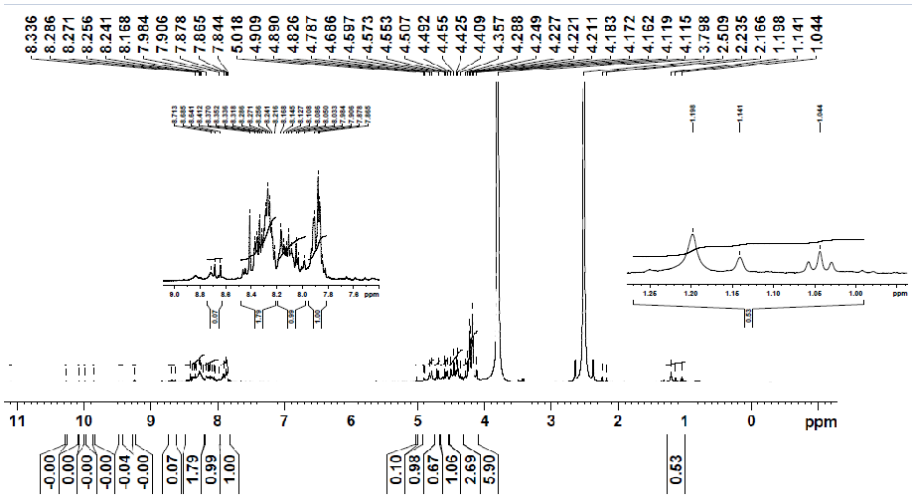

Figure 2: Proton NMR spectrum of R1.

Binding Aptitude Analysis Using UV–Titration Method

To 2.5 mL of $1X10^{-5}$ M R1 solution taken in the quartz cell, incremental additions of 20 µL of various metal salt solutions ($1X10^{-2}$ M) were added using micro pipette (during the titration) and the spectral changes were recorded for analysis. Alcoholic solutions of Pb, Cd & Mn salts and acetonitrile solutions of Hg, Ni & Cu salts were used in titration studies. UV-visible spectrum of R1 in acetonitrile had a peak at 258 nm and two shoulders near 300 nm and 358 nm. In ethanol medium two peaks are visible at 241 nm, 313 nm and a shoulder at 354 nm (Figure 3a&3b). Aromatic ring transitions (π-π*) were assigned (33) for UV region shoulders and peaks and an intramolecular charge transfer transition (34) was allocated for visible region shoulder.

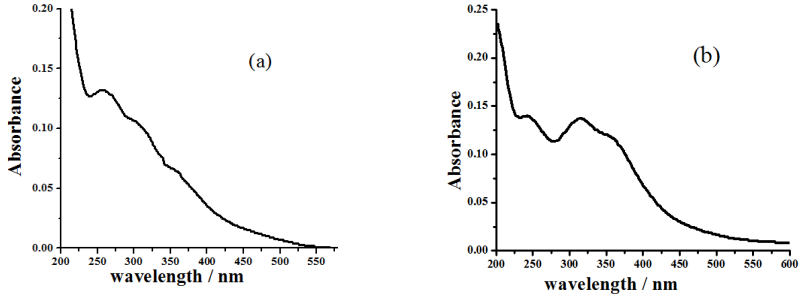

Figure 3: Electronic spectrum of R1 in **(a)** acetonitrile **(b)** ethanol.

Successive addition of Cu^{2+} ions drastically changed the spectrum of R1(Figure 4a) with the generation of MLCT band (Figure 4b) at 465 nm (35) accountable for the association of metal ion with receptor and disappearance of 258 nm peak with the transformation of 300 nm shoulder to a peak (Figure 4c) at 296 nm (blue-shift).

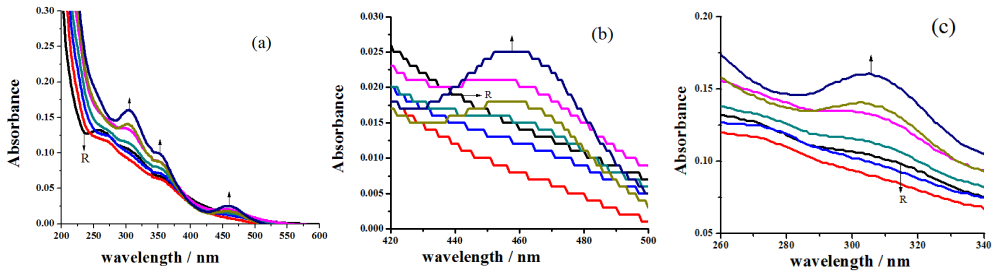

Figure 4: Spectral changes recorded for the addition of Cu^{2+} ions to R1 **(a)** Overall changes **(b)** MLCT band formation **(c)** conversion of shoulder in to peak.

Incremental addition of Hg^{2+} ions lead to the development of new peak around 237 nm (Figure 5a). Blue shift of 242 nm peak to 234 nm and 315 nm peak to 311 nm resulted from the addition of Pb^{2+} ions (Figure 5b). Red shift of 258 nm shoulder to 272 nm originated from the raise of Ni^{2+} ions (Figure 5c). Appreciable variations were recorded for the increase of Cd^{2+} & Mn^{2+} ions. Transformation of π-π* transition peaks of R1 upon the addition of various metal ion supposes that R1 is capable of sensing Cu^{2+}, Hg^{2+}, Ni^{2+}, Pb^{2+}, Cd^{2+} and Mn^{2+} ions.

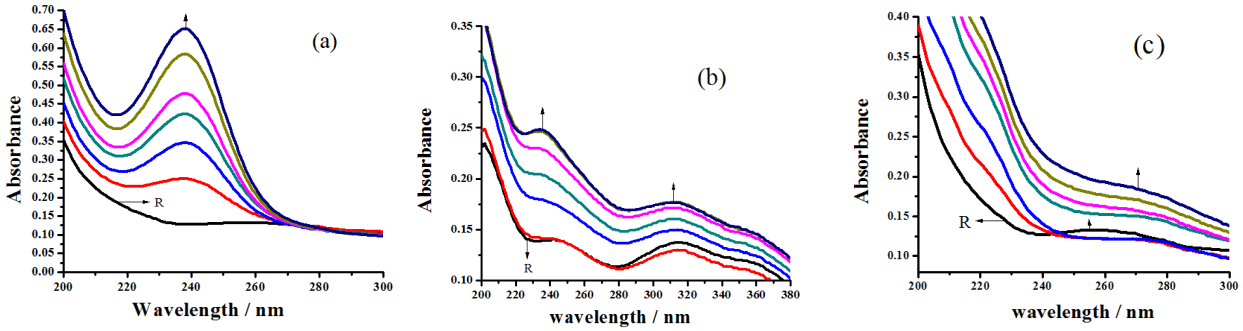

Figure 5: Spectral changes noticed in spectrum of R1 for the addition of **(a)** Hg^{2+} ions, **(b)** Pb^{2+} ions, **(c)** Ni^{2+} ions.

The presence of electron donating methyl group in the aromatic part substituted imine group, might cause the π-π* transition to happen meritoriously. This might be the reason for the appearance of prominent peak at 335 nm (Figure 6a) in acetonitrile medium and at 350 nm (Figure 6b) in ethanol. A shoulder at 310 nm was also recorded in alcoholic medium, in addition to the above mentioned peak.

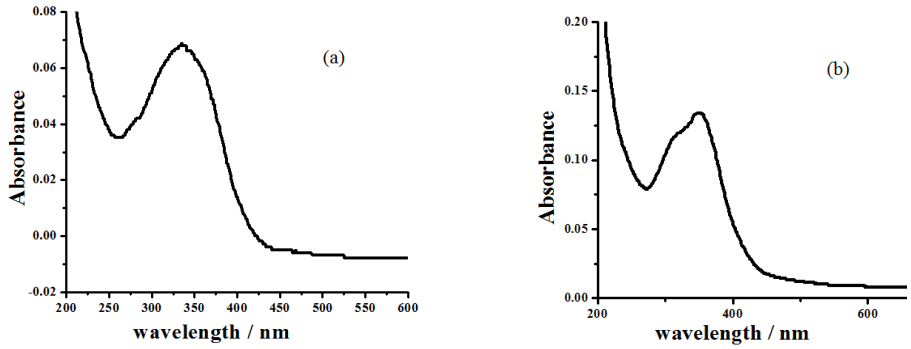

Figure 6: Electronic spectra of R1 in **(a)** acetonitrile, **(b)** ethanol.

Recognition ability of R2 towards Cu^{2+} ions was revealed by the formation of an MLCT band at 461 nm along with blue shift of 337 nm to peak 310 nm (Figure 7a). Locking attitude of R2 towards Hg^{2+} was revealed by the formation of new peak at 237 nm (Fig 7b). Disappearances of 337 nm peaks with simultaneous appearance of shoulder at 278 nm (Figure 7c) for the addition of Ni^{2+} ions also revealed the sensing ability of R2. Conversion of 357 nm peak to shoulder on increasing the concentration of Pb^{2+} ions and acceptable upsurge in the absorbance value of R2 for the cumulative addition of Mn^{2+} & Cd^{2+} also unveiled the binding aptitude of R2.

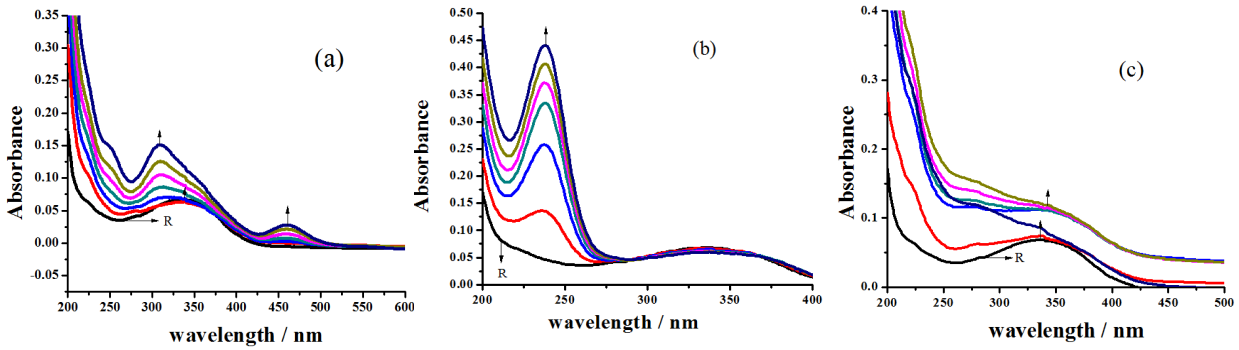

Figure 7: Spectral changes noticed in the spectrum of R2 for the addition of **(a)** Cu^{2+} ions, **(b)** Hg^{2+} ions, **(c)** Ni^{2+} ions.

Assessment of Concentration Required for Effective Sensing

The required concentration for the recognition of metal ions by the newly synthesized sensor was calculated from the anodic current value observed for the oxidation peak realized for the applied potential under anaerobic conditions. In Figure 8, cyclic voltammograms of R1 ($1X10^{-3}$ M) recorded for different scan rates (20, 50 & 100 mV/s) were presented. The calculated values of I_{pa} , I_{pc}, and ΔE_P are presented in Table 1. The ΔE_P (132- 219 mV) values derived from the anodic and cathodic potential data were greater than the expected 59 mV of a reversible process (36).

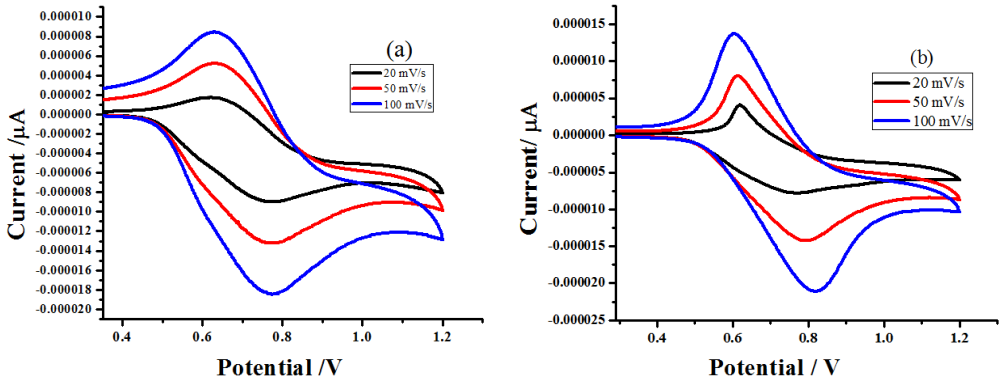

Figure 8: CV of R1 with different scan rate in **(a)** acetonitrile and **(b)** ethanol.

Table 1: Electrochemical parameters of R1 ($1X10^{-3}$M).

Scan Rate- mV/ sec	E_{pa} (V)	E_{pc} (V)	ΔE_p (V)	$E_{1/2}$ (V)	I_{pa} x10^{-6} (µA)	I_{pc} x10^{-6} (µA)
Solvent –Acetonitrile						
20	0.765	0.631	0.134	0.698	-0.914	1.709
50	0.765	0.629	0.136	0.697	-1.322	5.303
100	0.774	0.627	0.147	0.71	-1.841	8.503
Solvent – Ethanol						
20	0.766	0.619	0.147	0.692	-0.788	4.002
50	0.793	0.613	0.18	0.703	-1.414	8.027
100	0.820	0.601	0.219	0.710	-2.124	13.760

CV titration studies were carried out by adding 20 µL of either $1X10^{-3}$ M or $1X10^{-1}$ M metal salts' solution to 10 mL of 1X 10^{-3} molar R1 solution taken in the three-compartment cell. The registered cyclic voltammograms had a varied amount of positive potential shift for oxidation peak and a negative potential shift for reduction peak, which unveiled the different metal ion sensing nature of newly synthesized receptors (37, 38). Voltammograms recorded for the addition of Cd^{2+} ions are presented in Figure 9.

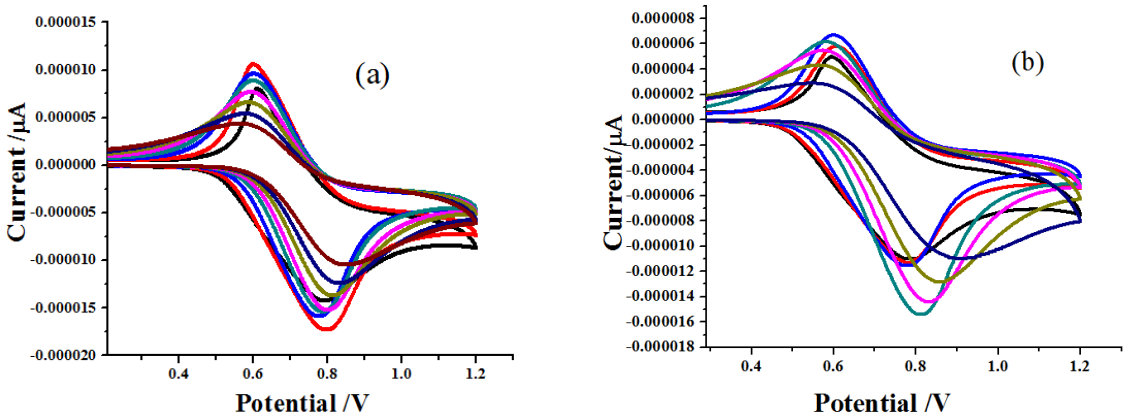

Figure 9: Deviations in the voltammogram of R1 for the addition of Cd^{2+} ions, **(a)** $1X10^{-3}$ M, **(b)** $1X10^{-1}$ M.

Electronic configuration of the metal ion may affect its binding nature to the receptor. The difference in the I_{pa} and ΔE_p values (Table 2) observed for the varied metal ions with $1X10^{-3}$ M concentration (Figure 10) matched with the above expectation. The repulsive force operating between metal cation and oxidized ferrocene unit was also a reason for the noticed variations in the I_{pa} & ΔE_p (39). The order of binding of R1 estimated from the ΔI_{pa} (%), deliberated from the I_{pa} amount detected for the oxidation wave of sensor's solution and different metal ions added to it, was Cd, 86.5%>Ni, 33.2%>Hg, 24.6%>Pb, 13.6%>Mn, 8.4%>Cu, 3.9%.

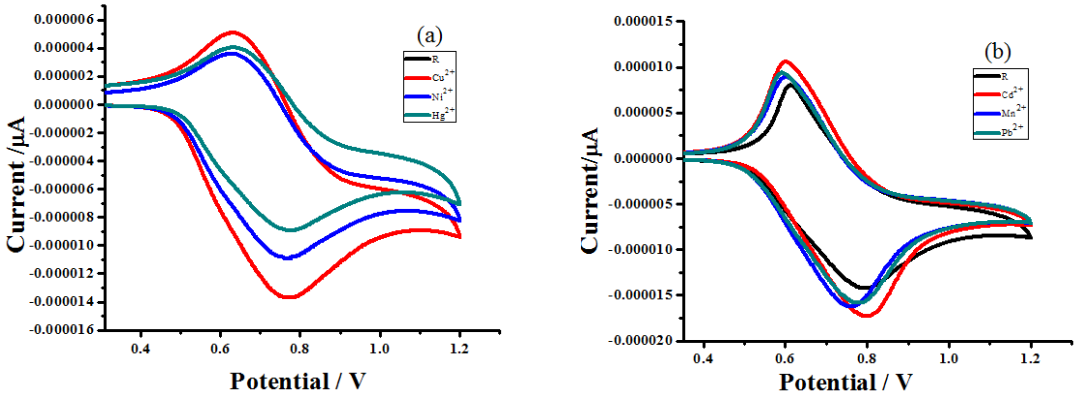

Figure 10: CV of R1 ($1X10^{-3}$ M) with dissimilar metal ions ($1X10^{-3}$ M) in **(a)** acetonitrile and **(b)** ethanol [at 50 mV/s scan rate].

Table 2: CV data for the addition of dissimilar metal ions under equimolar conditions [at 50 mV/s scan rate].

Addition	E_{pa} (V)	E_{pc} (V)	ΔE_p (V)	$E_{1/2}$ (V)	I_{pa} x10^{-5} (μA)	I_{pc} x10^{-6} (μA)
Solvent - Acetonitrile						
Receptor	0.765	0.629	0.136	0.697	-1.322	5.303
Cu^{2+}	0.767	0.635	0.132	0.701	-1.380	5.091
Ni^{2+}	0.765	0.633	0.132	0.699	-1.087	3.539
Hg^{2+}	0.775	0.637	0.138	0.706	-8.917	3.998
Solvent - Ethanol						
Receptor	0.793	0.613	0.18	0.703	-1.414	8.027
Cd^{2+}	0.794	0.598	0.196	0.696	-1.743	1.078
Mn^{2+}	0.757	0.602	0.155	0.679	-1.638	8.769
Pb^{2+}	0.778	0.596	0.182	0.687	-1.586	9.293

The order of sensing power of R1 under multimolar conditions (1X10^{-3} M, R1/1X10^{-1} M, Mn^{2+}), derived from the ΔI_{pa} (%), which in turn were calculated from the I_{pa} values (Table 3), was Mn, 59.3%>Pb, 44.3%>Cd, 27.1%>Cu, 15.9%>Ni, 2.9%>Hg, 1.8%. Appraisal of binding order of R1 under dissimilar concentrations of metal ion revealed that R1 was more potent than Cd, Ni, and Hg ions at lower concentrations, and dominant over Mn, Pb, and Cd at higher concentrations (Figure 11).

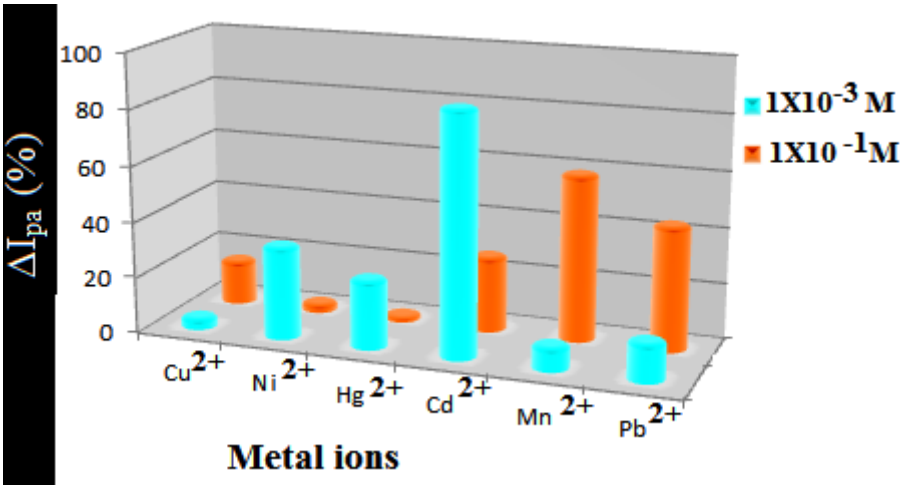

Figure 11: Chart showing the concentration required and sensing ability of R1.

Table 3: CV data for the addition of dissimilar metal ions under multimolar conditions [at 50 mV/s scan rate].

Addition	E_{pa} (V)	E_{pc} (V)	ΔE_p (V)	$E_{1/2}$ (V)	I_{pa} x10^{-5} (µA)	I_{pc} x10^{-6} (µA)
Solvent – Acetonitrile						
Receptor	0.765	0.629	0.136	0.697	-1.322	5.303
Cu^{2+}	0.798	0.666	0.132	0.732	-1.282	4.457
Ni^{2+}	0.788	0.646	0.142	0.717	-1.328	5.145
Hg^{2+}	0.767	0.639	0.128	0.703	-1.202	5.205
Solvent - Ethanol						
Receptor	0.793	0.613	0.18	0.703	-1.414	8.027
Cd^{2+}	0.777	0.609	0.168	0.693	-1.134	5.845
Mn^{2+}	0.774	0.609	0.165	0.691	-8.161	3.264
Pb^{2+}	0.777	0.602	0.175	0.689	-1.096	4.470

Table 4: Electrochemical data of R2 ($1X10^{-3}$M) with different scan rates.

Scan Rate-mV/s	E_{pa} (V)	E_{pc} (V)	ΔE_p (V)	$E_{1/2}$ (V)	I_{pa} x10^{-5} (µA)	I_{pc} x10^{-6} (µA)
Solvent –Acetonitrile						
20	0.818	0.706	0.112	0.762	-6.934	1.240
50	0.827	0.704	0.123	0.765	-1.061	2.926
100	0.827	0.696	0.131	0.761	-1.473	5.551
Solvent – Ethanol						
20	0.657	0.601	0.056	0.629	-3.296	4.903
50	0.706	0.612	0.094	0.659	-6.096	1.754
100	0.736	0.605	0.131	0.670	-8.845	3.677

The change in trend of I_{pa}, I_{pc} & ΔE_p values assessed for R2 (Table 4) with different scan rate are similar to the behavior of R1.

Concentration assessment experiment of R2 was also carried out using the same method adopted for R1. The order of binding ability of R2 estimated from ΔI_{pa} (%) values under homo-molar concentrations was Ni, 48.7%>Hg, 37.8%>Pb, 34.2%>Mn, 24.5%>Cd, 8.6>Cu, 6.8% (Table 5), and at hetero-molar conditions was (Ni, 46.1%>Cd, 37.3%>Cu, 34.1%>Pb, 29.3%>Hg, 26.8%>Mn, 0.0%) (Table 6). The pictorial presentation of the role of metal ion concentration required for effective sensing of R2 is given in Figure 12.

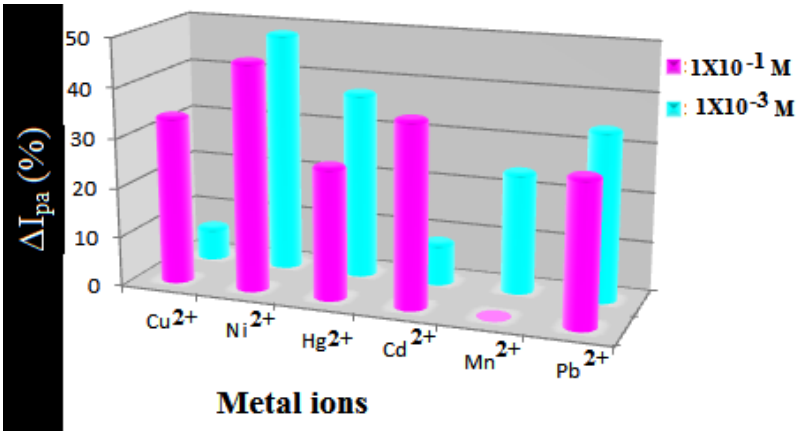

Figure 12: Chart showing the concentration required and sensing ability of R2.

Table 5: CV data for the addition of dissimilar metal ions under homo-molar conditions [at 50 mV/s scan rate].

Addition	E_{pa} (V)	E_{pc} (V)	ΔE_p (V)	$E_{1/2}$ (V)	I_{pa} x10^{-5} (μA)	I_{pc} x10^{-6} (μA)
Solvent – Acetonitrile						
Receptor	0.827	0.704	0.123	0.765	-1.061	2.926
Cu^{2+}	0.814	0.706	0.108	0.76	-1.075	2.727
Ni^{2+}	0.758	0.625	0.133	0.691	-5.056	5.741
Hg^{2+}	0.814	0.702	0.112	0.758	-1.530	4.705
Solvent - Ethanol						
Receptor	0.706	0.612	0.094	0.659	-6.096	1.754
Cd^{2+}	0.728	0.616	0.112	0.672	-5.855	1.920
Mn^{2+}	0.775	0.580	0.195	0.677	-1.151	2.326
Pb^{2+}	0.741	0.597	0.144	0.669	-6.525	1.154

Table 6: CV data for the addition of dissimilar metal ions under heteromolar conditions [at 50 mV/s scan rate].

Addition	E_{pa} (V)	E_{pc} (V)	ΔE_p (V)	$E_{1/2}$ (V)	I_{pa} x10^{-5} (μA)	I_{pc} x10^{-6} (μA)
Solvent – Acetonitrile						
Receptor	0.827	0.704	0.123	0.765	-1.061	2.926
Cu^{2+}	0.811	0.666	0.145	0.738	-7.4381	1.926
Ni^{2+}	0.784	0.666	0.118	0.738	-6.633	1.577
Hg^{2+}	0.791	0.676	0.115	0.733	-6.284	2.140
Solvent - Ethanol						
Receptor	0.706	0.612	0.094	0.659	-6.096	1.754
Cd^{2+}	0.762	0.587	0.175	0.674	-1.123	2.801
Mn^{2+}	-	-	-	-	-	-
Pb^{2+}	0.747	0.582	0.165	0.664	-8.372	1.239

CONCLUSION

The formation of unsymmetrical Schiff bases, when ferrocenecarboxaldehyde is present as one of the reactants, is barred due to the high reactivity of ferrocene component. Efforts made by our team resulted to the preparation, characterization, and exploration of the sensing ability of *N*'-((*E*)-4-nitrobenzylidene)-2-((*E*)-2-(ferrocenylidene)hydrazine-1-carbothiohydrazide and *N*'((*E*)-4-*N*,*N*-dimethylaminobenzylidene)-2-((*E*)-2-(ferrocenylidene) hydrazine-1-carbothiohydrazide. FTIR, ^{1}HNMR, and Mass spectral analyses materialize the characterization of the above compounds. Competency in identifying the ions of metals like Cu, Ni, Hg, Cd, Mn & Pb by the newly synthesized compound was realized in UV-Visible titration studies. The role of concentration on the sensing activity of the sensors R1 and R2 resulted from the anodic current values obtained in CV studies.

CONFLICTS OF INTEREST

The authors declare that there are no conflicts.

ACKNOWLEDGEMENT

The support extended by Dr. K. Pandian, Professor of Inorganic Chemistry, at the University of Madras is gratefully acknowledged. The research scholar, D.Saranya wishes to record her thanks to the State Government of Tamil Nadu, India for the annual research assistant grant.

REFERENCES

1a. Malik LA, Bashir A, Qureashi A, Pandith AH. Detection and removal of heavy metal ions: a review. Environ Chem Lett. 2019 Dec;17(4):1495–521. <DOI>. **1b.** Nagajyoti PC, Lee KD, Sreekanth TVM. Heavy metals, occurrence and toxicity for plants: a review. Environ Chem Lett. 2010 Sep;8(3):199–216. <DOI>.

2a. Bansod B, Kumar T, Thakur R, Rana S, Singh I. A review on various electrochemical techniques for heavy metal ions detection with different sensing platforms. Biosensors and Bioelectronics. 2017 Aug;94:443–55. <DOI>. **2b.** Gong T, Liu J, Liu X, Liu J, Xiang J, Wu Y. A sensitive and selective sensing platform based on CdTe QDs in the presence of l -cysteine for detection of silver, mercury and copper ions in water and various drinks. Food Chemistry. 2016 Dec;213:306–12. <DOI>.

3. Tian M, Fang L, Yan X, Xiao W, Row KH. Determination of Heavy Metal Ions and Organic Pollutants in Water Samples Using Ionic Liquids and Ionic Liquid-Modified Sorbents. Journal of Analytical Methods in Chemistry. 2019 Oct 31;2019:1–19. <DOI>.

4a. Zhang M, Shi J, Liao C, Tian Q, Wang C, Chen S, et al. Perylene Imide-Based Optical Chemosensors for Vapor Detection. Chemosensors. 2020 Dec 22;9(1):1. <DOI>. **4b.** Elke K, Jermann E, Begerow J, Dunemann L. Determination of benzene, toluene, ethylbenzene and xylenes in indoor air at environmental levels using diffusive samplers in combination with headspace solid-phase microextraction and high-resolution gas chromatography–flame ionization detection. Journal of Chromatography A. 1998 Nov;826(2):191–200. <DOI>.

5. Berhanu AL, Gaurav, Mohiuddin I, Malik AK, Aulakh JS, Kumar V, et al. A review of the applications of Schiff bases as optical chemical sensors. TrAC Trends in Analytical Chemistry. 2019 Jul;116:74–91. <DOI>.

6. Borah N, De S, Gogoi A, Das G. A series of benzothiazole-based Schiff bases for the colorimetric sensing of fluoride and acetate ions: acetate-induced turn-on fluorescence for selectivity. New J Chem. 2020;44(43):18703–13. <DOI>.

7. Abu-Dief AM, Mohamed IMA. A review on versatile applications of transition metal complexes incorporating Schiff bases. Beni-Suef University Journal of Basic and Applied Sciences. 2015 Jun;4(2):119–33. <DOI>.

8. Garza-Lombó C, Posadas Y, Quintanar L, Gonsebatt ME, Franco R. Neurotoxicity Linked to Dysfunctional Metal Ion Homeostasis and Xenobiotic Metal Exposure: Redox Signaling and Oxidative Stress. Antioxidants & Redox Signaling. 2018 Jun 20;28(18):1669–703. <DOI>.

9. Jain R, Singh SK, Advani U, Kohli S, Sharma N. Mercury toxicity and its management. Int Res J Pharm. 2013 Sep 9;4(8):38–41. <DOI>.

10. Farina M, Avila DS, da Rocha JBT, Aschner M. Metals, oxidative stress and neurodegeneration: A focus on iron, manganese and mercury. Neurochemistry International. 2013 Apr;62(5):575–94. <DOI>.

11. Qi X, Jun EJ, Xu L, Kim S-J, Joong Hong JS, Yoon YJ, et al. New BODIPY Derivatives as OFF–ON Fluorescent Chemosensor and Fluorescent Chemodosimeter for Cu $^{2+}$: Cooperative Selectivity Enhancement toward Cu $^{2+}$. J Org Chem. 2006 Mar 31;71(7):2881–4. <DOI>.

12. Taylor AA, Tsuji JS, Garry MR, McArdle ME, Goodfellow WL, Adams WJ, et al. Critical Review of Exposure and Effects: Implications for Setting Regulatory Health Criteria for Ingested Copper. Environmental Management. 2020 Jan;65(1):131–59. <DOI>.

13. Bao J, Xing Y, Feng C, Kou S, Jiang H, Li X. Acute and sub-chronic effects of copper on survival, respiratory metabolism, and metal accumulation in Cambaroides dauricus. Sci Rep. 2020 Dec;10(1):16700. <DOI>.

14. Brewer GJ. Copper toxicity in the general population. Clinical Neurophysiology. 2010 Apr;121(4):459–60. <DOI>.

15. Chakraborty S, Rayalu S. Detection of nickel by chemo and fluoro sensing technologies. Spectrochimica Acta Part A: Molecular and Biomolecular Spectroscopy. 2021 Jan;245:118915. <DOI>.

16. Song X, Fiati Kenston SS, Kong L, Zhao J. Molecular mechanisms of nickel induced neurotoxicity and chemoprevention. Toxicology. 2017 Dec;392:47–54. <DOI>.

17. Das KK, Reddy RC, Bagoji IB, Das S, Bagali S, Mullur L, et al. Primary concept of nickel toxicity – an overview.

Journal of Basic and Clinical Physiology and Pharmacology. 2019 Mar 26;30(2):141–52. <DOI>.

18a. Erikson KM, Syversen T, Aschner JL, Aschner M. Interactions between excessive manganese exposures and dietary iron-deficiency in neurodegeneration. Environmental Toxicology and Pharmacology. 2005 May;19(3):415–21. <DOI>. **18b.** Peres TV, Aschner M. Nutritional, Genetic, and Molecular Aspects of Manganese Intoxication. In: Molecular, Genetic, and Nutritional Aspects of Major and Trace Minerals [Internet]. Elsevier; 2017 [cited 2022 Mar 11]. p. 367–76. <DOI>.

19. Harischandra DS, Ghaisas S, Zenitsky G, Jin H, Kanthasamy A, Anantharam V, et al. Manganese-Induced Neurotoxicity: New Insights Into the Triad of Protein Misfolding, Mitochondrial Impairment, and Neuroinflammation. Front Neurosci. 2019 Jun 26;13:654. <DOI>.

20. Peres TV, Schettinger MRC, Chen P, Carvalho F, Avila DS, Bowman AB, et al. "Manganese-induced neurotoxicity: a review of its behavioral consequences and neuroprotective strategies." BMC Pharmacol Toxicol. 2016 Dec;17(1):57. <DOI>.

21. Peres TV, Aschner M. Nutritional, Genetic, and Molecular Aspects of Manganese Intoxication. In: Molecular, Genetic, and Nutritional Aspects of Major and Trace Minerals [Internet]. Elsevier; 2017 [cited 2022 Mar 11]. p. 367–76. <DOI>.

22. Guilarte TR. Manganese and Parkinson's Disease: A Critical Review and New Findings. Environ Health Perspect. 2010 Aug;118(8):1071–80. <DOI>.

23. Ashraf U, Kanu AS, Deng Q, Mo Z, Pan S, Tian H, et al. Lead (Pb) Toxicity; Physio-Biochemical Mechanisms, Grain Yield, Quality, and Pb Distribution Proportions in Scented Rice. Front Plant Sci [Internet]. 2017 Feb 28 [cited 2022 Mar 11];8. <DOI>.

24. Boskabady M, Marefati N, Farkhondeh T, Shakeri F, Farshbaf A, Boskabady MH. The effect of environmental lead exposure on human health and the contribution of inflammatory mechanisms, a review. Environment International. 2018 Nov;120:404–20. <DOI>.

25a. Wani AL, Ara A, Usmani JA. Lead toxicity: a review. Interdisciplinary Toxicology. 2015 Jun 1;8(2):55–64. <DOI>. **25b**. Mani MS, Nayak DG, Dsouza HS. Challenges in diagnosing lead poisoning: A review of occupationally and nonoccupationally exposed cases reported in India. Toxicol Ind Health. 2020 May;36(5):346–55.

26. Genchi G, Sinicropi MS, Lauria G, Carocci A, Catalano A. The Effects of Cadmium Toxicity. IJERPH. 2020 May 26;17(11):3782. <DOI>.

27. Rafati-Rahimzadeh M, Rafati-Rahimzadeh M, Kazemi S, Moghadamnia A. Cadmium toxicity and treatment: An update. Caspian J Intern Med [Internet]. 2017 Jun [cited 2022 Mar 11];8(3): 135-45. <DOI>.
28. Rani A, Kumar A, Lal A, Pant M. Cellular mechanisms of cadmium-induced toxicity: a review. International Journal of Environmental Health Research. 2014 Jul 4;24(4):378–99. <DOI>.

29a. A. Metwally M, E. Khalifa M, Koketsu M. Thiocarbohydrazides: Synthesis and Reactions. Chemistry. 2012 Aug 31;2(2):38–51. <DOI>. **29b.** Andleeb H, Hussain M, Abida Ejaz S, Sevigny J, Farman M, Yasinzai M, et al. Synthesis and computational studies of highly selective inhibitors of human recombinant tissue non-specific alkaline phosphatase (h-TNAP): A therapeutic target against vascular calcification. Bioorganic Chemistry. 2020 Aug;101:103999. <DOI>.

30a. Constantinescu C, Matei A, Ion V, Mitu B, Ionita I, Dinescu M, et al. Ferrocene carboxaldehyde thin films grown by matrix-assisted pulsed laser evaporation for non linear optical applications. Applied Surface Science. 2014 May;302:83–6. <DOI>. **30b.** Bodenheimer JS, Low W. A vibrational study of ferrocene and ruthenocene. Spectrochimica Acta Part A: Molecular Spectroscopy. 1973 Sep;29(9):1733–43. <DOI>.

31. Gryaznova TP, Katsyuba SA, Milyukov VA, Sinyashin OG. DFT study of substitution effect on the geometry, IR spectra, spin state and energetic stability of the ferrocenes and their pentaphospholyl analogues. Journal of Organometallic Chemistry. 2010 Nov;695(24):2586–95. <DOI>.

32a. Çatıkkaş B. Raman and FT-IR Spectra, DFT and SQMFF calculations for N,N-Dimethylaniline. PEN [Internet]. 2017 Jun 24 [cited 2022 Mar 11];5(2):237-44. <DOI>. **32b**. Lu R, Gan W, Wu B, Zhang Z, Guo Y, Wang H. C−H Stretching Vibrations of Methyl, Methylene and Methine Groups at the Vapor/Alcohol (*n* = 1−8) Interfaces. J Phys Chem B. 2005 Jul 1;109(29):14118–29. <DOI>.
33. Barwiolek M, Kaczmarek-Kędziera A, Muziol TM, Jankowska D, Jezierska J, Bieńko A. Dinuclear Copper(II) Complexes with Schiff Bases Derived from 2-Hydroxy-5-Methylisophthalaldehyde and Histamine or 2-(2-Aminoethyl)pyridine and Their Application as Magnetic and Fluorescent Materials in Thin Film Deposition. IJMS. 2020 Jun 28;21(13):4587. <DOI>.

34. Benramdane R, Benghanem F, Ourari A, Keraghel S, Bouet G. Synthesis and characterization of a new Schiff base derived from 2,3-diaminopyridine and 5-methoxysalicylaldehyde and its Ni(II), Cu(II) and Zn(II) complexes. Electrochemical and electrocatalytical studies. Journal of Coordination Chemistry. 2015 Feb 1;68(3):560–72. <DOI>.

35a. Northcote-Smith J, Kaur P, Suntharalingam K. A Cancer Stem Cell Potent Copper(II) Complex with a *S* , *N* , *S* -Schiff base Ligand and Bathophenanthroline. Eur J Inorg Chem. 2021 May 14;2021(18):1770–5. **35b**. Ciesienski KL, Haas KL, Franz KJ. Development of next-generation photolabile copper cages with improved copper binding properties. Dalton Trans. 2010;39(40):9538. <DOI>.

36a. Kamatchi P, Selvaraj S, Kandaswamy M. Synthesis, magnetic and electrochemical studies of binuclear copper(II) complexes derived from unsymmetrical polydentate ligands. Polyhedron. 2005 Jun;24(8):900–8. <DOI>. **36b**. Samin AJ. A one-dimensional stochastic approach to the study of cyclic voltammetry with adsorption effects. AIP Advances. 2016 May;6(5):055101. <DOI>.

37a. Li M, Wang R. Synthesis and multi-response research of a highly selective fluorescent chemosensor for Zn^{2+}. IOP Conf Ser: Earth Environ Sci. 2017 Apr;61:012043. <URL>. **37b**. Miller SR, Gustowski DA, Chen Z, Gokel GW, Echegoyen L, Kaifer AE. Rationalization of the unusual electrochemical behavior observed in lariat ethers and other reducible macrocyclic systems. Anal Chem. 1988 Oct 1;60(19):2021–4. <DOI>.

38a. Alfonso M, Tárraga A, Molina P. Ferrocene-based multichannel molecular chemosensors with high selectivity and sensitivity for Pb(ii) and Hg(ii) metal cations. Dalton Trans. 2010;39(37):8637. <DOI>. **38b**. Medina JC, Goodnow TT, Rojas MT, Atwood JL, Lynn BC, Kaifer AE, et al. Ferrocenyl iron as a donor group for complexed silver in ferrocenyldimethyl[2.2]cryptand: a redox-switched receptor effective in water. J Am Chem Soc. 1992 Dec;114(26):10583–95. <DOI>.

39a. Kamal A, Kumar S, Kumar V, Mahajan RK. Selective sensing ability of ferrocene appended quinoline-triazole derivative toward Fe (III) ions. Sensors and Actuators B: Chemical. 2015 Dec;221:370–8. <DOI>. **39b**. Sanan R, Kang TS, Mahajan RK. Complexation, dimerisation and solubilisation of methylene blue in the presence of biamphiphilic ionic liquids: a detailed spectroscopic and electrochemical study. Phys Chem Chem Phys. 2014;16(12):5667. <DOI>.